CHAPTER V

TUNING THE SELECTIVE OF RING OPENING OF 1,3-DIMETHLCYCLOHEXANE WITH THE ADDITION OF POTASSIUM OVER Ir/SiO_2 CATALYSTS

5.1 Abstract

The catalytic properties of Ir/SiO_2 and K promoted Ir/SiO_2 for ring opening of 1,3-dimethylcyclohexane (1,3-DMCH) have been evaluated. Several ring opening mechanisms: dicarbene, adsorbed olefin or metallocyclobutane proceed on metal catalysts. In order to improve the cetane number, only the cleavage of C-C bond at substituted position via adsorbed olefin or metallocyclobutane mechanism which yields less branched chain hydrocarbon is required. In contrast, the breakage of C-C bond at unsubstituted position (secondary-secondary) ends up with a high degree of branched products which cause a decrease in cetane number. The present contribution shows that the selective of the opening of C-C bonds on Ir/SiO_2 can be tuned by varying K loading. The addition of potassium produced severe superficial changes that were reflected in catalytic activity and selectivity. It was found that the dispersions of Ir using CO adsorption slightly increased with rising K surface loading up to 2 wt.%. The result may due to the decease in Ir cluster or the K-Ir interaction that might facilitate the dissociative adsorption of hydrogen. In contrast, the Ir dispersion was drastically decreased due to the non-uniform decorative effect of potassium over Ir particles at higher K loading. It was postulated that most of the IrOx clusters were blocked. The promoted and unpromoted Ir catalysts were characterized by chemisorption of CO and H_2, temperature-programmed techniques, X-ray photoelectron spectroscopy (XPS), Extended X-ray absorption fine structure spectroscopy (EXAFS) and near-edge X-ray absorption fine structure spectroscopy (NEXAFS).

5.2 Introduction

In the United States, the Environment Protection Agency started implementing the Tier 2 Gasoline Sulfur Control Program for cleaner gasoline in 2004. This program limits the maximum sulfur level to 15 ppm by 2006. Additional specifications for minimum cetane index at 40 and maximum aromatics content at 35 vol.% will also be imposed. In order to meet the stringent environmental regulations on petroleum fuels, several approaches have been proposed. For instance, a process involving two consecutive steps, hydrogenation of the aromatics to saturated naphthenic compounds was combined with the traditional hydrocracking of the saturated rings [1]. However, excessive cracking to molecules with lower molecular weights is still in a challenging issue.

Recently, the increase in cetane number and the minimization of the loss of hydrocarbons through a selective ring opening (SRO) process were suggested [2-4]. The main goal of the SRO reaction is to convert naphthenic rings to paraffinic compounds with expectedly higher cetane number while to keep the same carbon number as the original naphthenic compounds. However, as we have pointed out in two naphthenic rings, the opening of only one ring would not result in a substantial gain in cetane number compared to that of fully hydrogenated molecule [5]. Conversely, if the second ring is continuously cleaved on a catalyst that favors the breakage of substituted tertiary-secondary endocyclic C–C bonds and some of them even more sterically hindered tertiary–tertiary C–C bonds, the cetane numbers of these products is considerably higher than that of the ones that break at secondary-secondary C-C bonds via either acid catalyzed or dicarbene mechanism [6]. This analysis suggests that the only successful strategy to significantly increase cetane number of decalin feedstocks should be based on a precisely tailored catalyst with high selectivity towards the cleavage of substituted endocyclic C–C bonds.

As pointed out by Gault (1981) and Maire and co-workers, the ring opening of naphthenic compounds over metal catalysts was proceeded via different mechanisms such as dicarbene, adsorbed olefin or metallocyclobutane [7-8]. The dicarbene mode was associated with breaking unsubstituted C-C bonds to produce branched molecules [9-13]. In the other two mechanisms, subsitituted C-C bonds

were preferentially broken resulting in alkane products with high linearity. The effect of metal particle size on Pt/Al_2O_3 catalysts for the ring opening of methylcylopentane was studied by Gault [7]. It was observed that on highly dispersed Pt on Al_2O_3, the breaking of any endocyclic C–C bonds followed the statistic number. This finding was attributed to a π-allyl mechanism that competes with the dicarbene mechanism. On the other hand, on Pt catalysts with larger metal clusters, secondary–secondary C–C bonds were preferentially broken. It is notable that the dicarbene mechanism was preferred when large ensembles were present. In order to explain the observed rupture of sterically-hindered substituted tertiary–secondary C–C bonds on these low dispersed Pt catalysts, the metallocyclobutane mechanism that competes with the dicarbene mechanism was proposed. Some good evidence that supports this proposed was given by Coq *et al.*, (1995) and McVicker *et al.* ,(2002) for the hydrogenolysis of 1,2,4 trimethyl-cyclohexane and 2,2,3,3-tetramethylbutane, respectively [3, 14].

The outstanding hydrogenolysis activity of Ir metal compared to other group VIII transition metals was found in many previous works [15-18]. Most recently, we reported that the preferred pathway of ring opening of 1,2- and 1,3-dimethylcyclohexane on TiO_2-, Al_2O_3- and SiO_2-supported Ir catalysts appears to be related to a support effect rather than to an effect of metal dispersion [19]. In recent publications and a series of patents, McVicker *et al.* reported the high ring opening activity of Ir catalysts on six-membered naphthenic rings [3, 20-22]. They observed that the dicarbene mode was strongly favorable on Ir catalysts. Due to the fact that a successful strategy to improve CN of feedstocks should be based on a precisely tailored catalyst with high selectivity towards the cleavage of substituted endocyclic C–C bond, therefore the metallocyclobutane or adsorbed olefin is considered to meet this target.

Hoost and Goodwin study the modified catalyst using alkali ion, potassium (K) on Ru/SiO_2, to decrease the apparent activation energy and increased the apparent hydrogen reaction order for ethane hydrogenolysis [23]. Furthermore, Kazi *et al.*, (1995) decreased the H_2 adsorption strength and enhanced CO adsorption when Pd/SiO_2 was modified with Li ions [24]. Furthermore, the hydrogenation and hydrogenolysis activities were decreased with increasing Li loadings. Most recently, Pedrero *et al.* studied the oxidation of CO in H_2-CO mixtures using alkali promoter-

modified Pt/SiO_2 catalysts [25]. They found that alkali cations (e.g. Na, Rb, and Cs) not only improved the metal dispersion and titrated silanol groups (Si-OH) but also inhibited spillover-mediated H_2 oxidation pathways that decreased CO oxidation. From these results we can envisage that the addition of alkali ions to SiO_2-supported metal catalysts changes both the hydrogen transfer reactions and the ensemble of atoms (metal dispersion). This might affect the adsorption mode of the model molecule and therefore the reaction pathways.

In the present paper, we investigated the effects of different potassium loadings as promoter into Ir/SiO_2 on the ring opening reaction of 1,3-dimethylcyclohexane. We also fully characterized the series of catalysts in order to gain insight into the relationship between the catalyst surface properties and the selectivity ring opening products of Ir-containing catalysts.

5.3 Experimental

5.3.1 Catalyst Preparation

A series of supported 1 wt% Ir-containing catalysts were prepared by incipient wetness impregnation. Silica was impregnated with aqueous solutions of $IrCl_3.3H_2O$ (Alfa-Aesar, 99.9 %) at appropriate Ir concentrations to obtain 1 wt% loading, maintaining a liquid/solid ratio of 1.2 mL/g. The support material was silica (HiSil-210; PPG) with a BET surface area of 250 m^2/g. After impregnation, the catalyst precursors were dried overnight at 393 K and then calcined at 573 K for 2 h in flowing air.

5.3.2 Catalyst Characterization

5.3.2.1 Elemental Analysis

Semi-quantitative elemental ratio was verified by energy-dispersive X-ray spectroscopy (EDXS) in fairly good agreement with the nominal composition, using a Kevex model Delta-3 system connected to a JEOL JSM-880 scanning electron microscope. The emission peaks from the regions related to O(Kα), Si(Kα), K(Kα) and Ir(Lα) were recorded for each sample.

5.3.2.2 Chemisorption of CO

Reversible and irreversible CO uptakes at 300 K were measured by the volumetric technique. Catalysts (ca. 0.50 g) were treated in H_2 at 723 K for 2 h and then evacuated at the same temperature for 0.5 h before the chemisorption measurements were obtained. After treatment, the samples were cooled down to 300 K, and the first chemisorption isotherm was measured at 1–100 Torr. A second isotherm was obtained after the sample was evacuated at 300 K for 0.5 h. These two isotherms were extrapolated to zero adsorbate pressure and their difference was defined as the irreversible chemisorbed CO and used to calculate the reported CO/Ir values.

5.3.2.3 Temperature Programmed Reduction (TPR)

The samples were pre-treated before being analyzed with a 25 cm^3/min dry air flow rate to 573 K for 1 h. The TPR profiles were carried out by passing a continuous flow of 5 vol.% H_2-Ar mixture over 100 mg of in situ pretreated catalysts at a flow rate of 20 cm^3/min. The temperature was linearly increased at a heating rate of 10 K/min. The hydrogen uptake change against the temperature was monitored using a thermal conductivity detector (TCD), SRI model 110 TCD.

5.3.2.4 X-ray Photoelectron Spectroscopy

X-ray photoelectron spectroscopy (XPS) data were recorded at room temperature via a Physical Electronics PHI 5800 ESCA System with monochromatic Al Kα X-rays (1486.6 eV) operated at 100 W and 15 V in a chamber pressure of approximately 2.0×10^{-9} Torr. A 400 μm spot size and 58.7 eV pass energy were typically used for the analysis. Sample charging during the measurement was compensated by an electron flood gun. The electron take-off angle was 45° with respect to the sample surface. The reduction or the reaction of the samples was performed in a packed bed micro-reactor with an on/off valve on the top and bottom of the reactor. The reactor with the sample under He was transferred to a glove bag; the sample (in powder form) was placed in a stainless steel holder and it was kept in a vacuum transfer vessel (model 04-110A from Physical Electronics) to avoid any exposure to the atmosphere before the analysis. The energy scale of the instrument was calibrated using the Ag 3d5/2 line at binding energy of 368.3 eV. The

XPS data from the regions related to the C (1s), O (1s), Ir (4f), K (2p) and Si (2p) core levels were recorded for each sample. Quantification of the surface composition was carried out by integrating the peaks corresponding to each element with aid of the Shirley background subtraction algorithm, and then converting these peak areas to atomic composition by using the sensitivity factors provided for the each element by the PHI 5800 ESCA system software.

5.3.2.5 Extended X-ray Absorption Fine Structure (EXAFS) and Near Edge X-ray Absorption Fine Structure (NEXAFS)

The fine structure oscillations of each spectrum were isolated using the ATHENA program. The data were then fitted using the ARTHEMIS program in R-space between 1.8 and 3.1 Å to determine interatomic distances and coordination numbers. Backscattering amplitudes and phase shifts of theoretical standards were generated with the use of FEFF6.0 algorithm [28, 29]. As an ab initio calculation, FEFF uses a list of atomic coordinates in a cluster and physical information about the system such as type of absorbing atom and excited core-level for its calculation. In our case, the list of atomic coordinates was simplified using ATOMS which generates the required coordinates starting from a crystallographic description of the metallic Ir system [30].

Extended X-ray absorption fine structure (EXAFS) and near-edge X-ray absorption fine structure (NEXAFS) spectra of the Ir L3 edge (11215 eV) were recorded at the 2.3 beamline of the SSRL (Stanford Synchrotron Radiation Laboratory) in transmission mode using a Si (111) double-crystal monochromator. Spectra were taken using an in situ cell, which has been described previously [26, 27]. Samples were held within a 0.8-mm i.d. quartz capillary with 0.1-mm-thick walls. Gases were metered with electronic mass flow controllers. Ir catalysts were exposed to H_2 at 723 K, and reduction process was monitored from X-ray absorption near-edge spectra (XANES); we determined the extent of reduction by monitoring changes in the white line intensity. When the intensity of the white line remained unchanged, catalyst was cooled down to room temperature in H_2 and EXAFS spectra were taken.

5.3.3 Catalytic Activity Measurement and Data Analysis

The ring opening reaction of 1,3-dimethylcyclohexane (DMCH) (obtained from Sigma-Aldrich, 99 %) was carried out at 593 K under a total pressure of 3540 kPa, maintaining a molar ratio of hydrogen to hydrocarbon of 30. The runs were conducted in a plug-flow reactor consisting of a 1/2-inch stainless steel tube placed inside an electric furnace equipped with a three-zone temperature controller. Before each run, the catalyst was prior reduced at 723 K for 1.5 h and then cooled to the reaction temperature. Hydrogen and liquid hydrocarbon were brought in contact in the co-current mode. The liquid was continuously fed into the reactor using an Isco LC-5000 high-pressure pump operating in the volumetric flow rate range of 0.15–400 mL/h. This study was conducted at high pressure, high hydrogen to hydrocarbon ratio for which the catalyst deactivation is negligible. The products were collected as liquid in a dry ice contained acetone bath, with the temperature kept at 197 K to capture all of the products. The liquid product was manually injected into a Hewlett-Packard 5890 Plus GC for composition analysis. A Shimadzu GC-MS-QP5000 was used to identify the products with maximum certainty. Analysis of the numerous products obtained in this conversion was not straightforward, and many standard compounds were used to confirm the identity of the compounds.

5.4 Results and Discussion

5.4.1 Characterization

5.4.1.1 Metal Dispersion and Particle Size of Ir Catalysts

Compositions and metal dispersions of the potassium ions-promoted Ir SiO_2-supported catalysts were listed in Table 5.1. The metal dispersions slightly increased with increasing K loading until the K of 2 wt.% then the dispersions continuously decreased with higher K loadings. It seems that the slight presence of K improves metal dispersions according to the study of alkali ions in previous reports [31-33]. At significant K loading, hydrogen and CO uptakes decreased due to the blocking effect of potassium on Ir particles.

Table 5.1 Compositions, metal dispersion of Ir/SiO_2 and $Ir-K/SiO_2$ catalysts

K loading (wt.%)	Catalyst	CO/Ir[a]	N_{Ir-Ir}[b]
0	Ir/SiO_2	0.58	11.3
0.5	$Ir-0.5K/SiO_2$	0.61	10.8
1.3	$Ir-1.3K/SiO_2$	0.66	-
2.0	$Ir-2.0K/SiO_2$	0.66	9.6
3.0	$Ir-3.0K/SiO_2$	0.70	-
5.0	$Ir-5.0K/SiO_2$	0.52	-

[a] Chemisorption data obtained at 300 K after reducing the samples at 723 K.

[b] Average coordination number (N) and metal particle size (d_p) determined by EXAFS.

5.4.1.2 Temperature Programmed Techniques

Temperature-programmed reduction (TPR) profiles of catalysts prepared are illustrated in Figure 5.1. The TPR profile of the unmodified Ir/SiO_2 catalyst has shown two hydrogen-consumption peaks. The shoulder peak and the main peak attributed to the reduction of different nano-aggregate states of IrOx species on the silica surface or two morphologically different particles of iridium oxide at 534 K and 605 K, respectively [34, 35]. As the increase in K loading up to 2%, the major reduction step was shifted to lower reduction temperatures. Further promoter loadings caused an opposite behavior on this peak position. On the other hand, a small hydrogen uptake at higher temperatures (i.e. ~740 K) did become not only more intense with increasing potassium loading, but also more complex since several reduction steps were defined in the TPR profile of 5 wt.% modified-Ir/SiO_2 catalyst. The dependence of the major reduction steps with potassium content indicated that low loadings of potassium markedly promoted the reducibility of iridium oxide, probably due to a K-Ir interaction that facilitates the dissociative adsorption of hydrogen. Indeed, the effect of this promoter on the reducibility of metal oxides has been previously reported [36, 37]. However, potassium contents greater than 1.3 wt.% blocked most of the IrOx clusters thus inhibited the reaction of reduction. In consequence, the higher temperature required for reducing the oxide particles.

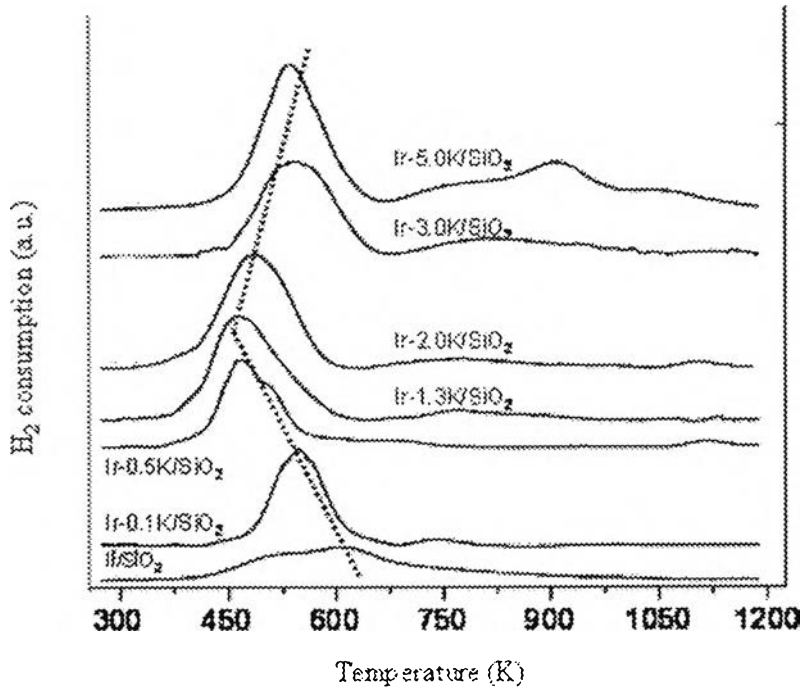

Figure 5.1 Temperature programmed reduction profiles of the catalytic precursors of potassium (K) promoted Ir/SiO_2 catalysts.

5.4.1.3 X-ray Photoelectron Spectroscopy

Binding energies (BEs) of core-level electrons and metal surface composition were obtained by X-ray Photoelectron Spectroscopy (XPS). Table 5.2 summaries the observed binding energies of core levels for the studied catalyst series. The BE for Ir 4f7/2, Si 2p and O 1s peaks in the unpromoted Ir/SiO_2 catalyst are into the range of expected values for the corresponding Ir(0) and SiO_2, suggesting that a poor Ir-SiO_2 interaction is occurred and consequently a low metal dispersion is obtained, see Table 5.1 [38]. On the other hand, the addition of potassium produced a slight shift of BE towards lower values of approximately 0.1-0.3 eV for Ir 4f7/2 and 0.3-0.5 eV for O 1s with respect to the unpromoted catalyst, whereas a BE shifted towards higher values of approximately 0.6-0.4 eV for K 2p3/2 peak is illustrated, considering a BE for K 4p3/2 of 292.1 eV for 2 wt. % K/SiO_2. This trend suggests that a slight increase of electron density on the Ir clusters because of potassium ion additions be occurred. However, no systematic deviation of the

different binding energies with changing of potassium loadings is noticed as was previously observed for sodium ion-promoted Pd/SiO_2 catalysts [39, 40].

Table 5.2 Electron binding energies of the core levels for Ir 4f, K 2p and Si 2p in the K ion-promoted Ir/SiO_2 catalysts

	Binding Energies (+ 0.1 eV)			
Catalyst	Ir 4f7/2	K 2p3/2	Si 2p	O 1s
Ir/SiO_2	60.5	-	102.3	531.9
$Ir\text{-}0.5K/SiO_2$	60.4	292.7	102.2	531.5
$Ir\text{-}1.3K/SiO_2$	60.2	292.6	102.0	531.4
$Ir\text{-}2.0K/SiO_2$	60.3	292.7	102.1	531.4
$Ir\text{-}3.0K/SiO_2$	60.2	292.5	102.0	531.5
$Ir\text{-}5.0K/SiO_2$	60.2	292.6	102.0	531.6

It has been reported that metal to support atomic ratio obtained through XPS for supported metal catalysts can provide important information regarding the dispersion and even crystal size-morphology of the supported phase [41]. For Ir containing catalysts, XP spectroscopy has been employed for studying the effect of the support; reduction temperature and addition of promoters on the hydrogenation reactions, however there have been no reports about the influence of alkali metal ions on the metal dispersion [42, 43]. The Ir 4f7/2/Si 2p, K 2p3/2/Si 2p and K 2p3/2/Ir 4f7/2 atomic surface ratios are fairly similar to the bulk atomic ratios, indicating that the catalyst components are well distributed.

5.4.1.4 Extended X-ray Absorption Fine Structure and Near Edge X-ray Absorption Fine Structure

The Fourier transform intensities of the weighted EXAFS functions $k3\chi(k)$ are shown in Figure 5.2 for K-promoted Ir/SiO_2 catalyst series. The higher-shell features are similar to iridium foil thus indicating the possible existence of clustered Ir atoms. All Fourier transformed spectra are consistent with an fcc-structure retained in the nanoparticles. The Fourier transform is an offset radial distribution diagram of the atoms surrounding the central absorber and also calculated from the interference pattern of the x-ray photo-electron wave as it passes

through the crystal media. As the Fourier transform is scaled to the coordination number this makes it possible to then visually determine changes in the chemical state through observing the changes in intensity. In the EXAFS analysis the finite nanoparticle size is reflected in the reduced average coordination number resulting from their considerable surface-area-to-volume ratio. As shown in Table 5.3, the Ir clusters in the supported samples have a reduction of Ir-Ir coordination number as a function of K-loading. Due to the small variation of the coordination number at nano-cluster diameters >2 nm and the errors associated with the EXAFS coordination number only approximate information about nanocluster sizes can be obtained by EXAFS and thus other measurements are essential for a comprehensive characterization of the nano-clusters as a function of size. With a hemispherical cuboctahedron fcc model, the Ir particle size can be roughly estimated to be about 3.7 nm for Ir/SiO_2, 2.2 nm for 0.5 wt.% K and 0.9 nm for 2 wt.% K, respectively [44]. This intensity reduction is predominantly caused by the decrease in the average first shell coordination number that results from the changing ratio of surface to bulk-like atoms in the clusters. It is clear that there is a striking decrease in Ir cluster size with increasing K loading in line with the above mentioned trend of the metal dispersion. Additionally, a significant bond length contraction with respect to the Ir foil can be observed, the first Ir-Ir coordination bond distances shrink with increased K loading. The relative first nearest Ir-Ir length contraction changes as a function of the inverse nano-cluster diameter. It should be noted that the bond lengths obtained from EXAFS results are the average. The noticeable decrease in lattice constants of supported Ir cluster can be understood in terms of a simple liquid drop model where enhanced surface energy is a main reason for the contracted lattice (nanosize effect) [45]. In response to the compressive tension, the atomic positions of the surface atoms should shift away from ideal sites and toward the cluster's core. Therefore these surface atoms should have a shorter the Ir-Ir coordination distance [46]. These results point out, adding K might wet the SiO_2 surface through an anchoring effect of the silanol groups with K ions and consequently the dispersion of Ir on SiO_2 surface enhances owing to the K^+ moisture-Ir interaction.

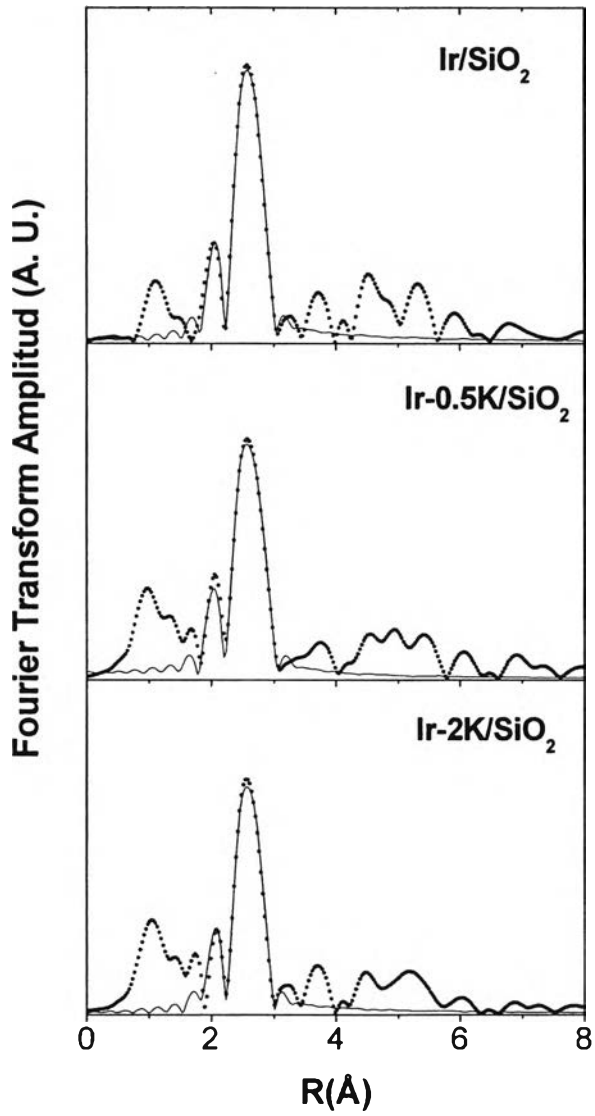

Figure 5.2 Amplitudes of the Fourier transforms of EXAFS data of samples measured in H_2 at room temperature after reduction at 723 K. Solid lines show the corresponding Fourier transforms of the fitted functions.

Table 5.3 Structural parameters of iridium obtained from fitting of EXAFS data using theoretical references developed with FEFF

Catalyst	<N>[a]	R[Å][b]	cσ2 [Å-2][c]	E_0 [eV] [d]
Ir/SiO_2	11.3±1	2.708(8)	0.0047(8)	7.3±1
$Ir\text{-}0.5K/SiO_2$	10.8±1	2.703(5)	0.0049(5)	7.5±1
$Ir\text{-}2.0K/SiO_2$	9.6±1	2.702(4)	0.0050(5)	7.0±1

[a] Average coordination numbers

[b] Bond distances

[c] Debye–Waller factors

[d] E_0 shift

A proposed schematic model of $Ir\text{-}K/SiO_2$ catalysts is illustrated in Figure 5.3, which is clearly illustrated the reduction of particle size in the presence of K ions and the partial coverage of metal particles by free potassium ion moistures.

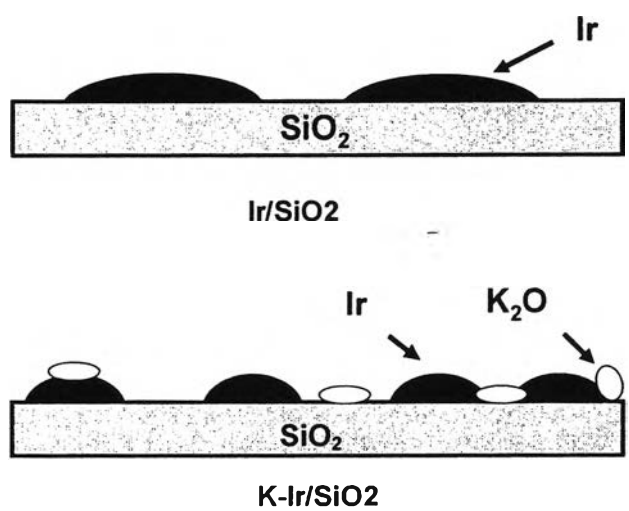

Figure 5.3 Surface representation of the potassium influence over silica-supported Ir particles.

5.4.2 Catalytic Activity

The primary products from RO of 1,3-DMCH are 2-methylheptane (2-MC7), 4-methylheptane (4-MC7) and 2,4-dimethylhexane (2,4-DMC6) which are designated in scheme 5.1 as products resulting from C-C cleavage at positions a, b, and c respectively. The breakage of the C-C bond at substituted position (tertiary-secondary C-C) resulted in low branched chain hydrocarbons which are 2-MC7 and 4-MC7 while the breakage of the C-C bond at unsubstituted position yielded high branched chain product which is 2,4-DMCH6. In a recent contribution, we predicted the cetane number of the primary products from the cleavage at a, b, and c using artificial neural network and a database of all of the available experimental cetane number data [5]. These estimations indicate that only low branched molecules (i.e., low CH_3/CH_2 ratio), 2MC-7 and 4-MC7, present significantly high cetane number compared to original reactant [47].

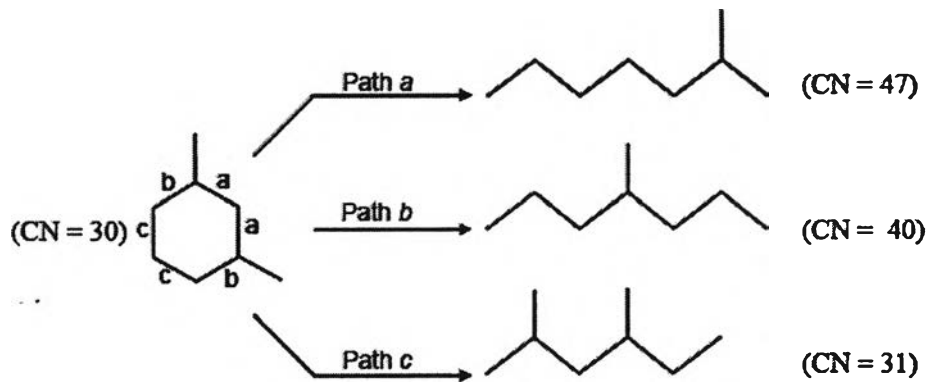

Scheme 5.1 Cetane numbers and reaction pathways for the primary products from ring opening reaction of 1,3-DMCH.

At low conversion, the primary products were mainly observed. Then these products continuously cracked to secondary products which resulted in the loss in carbon number at higher conversion such as 2-methylhexane (2-MC6), 3-methylhexane (3-MC6) and 2,4-dimethylpentane (2,4-DMC5). In this study, the products from isomerization were not found due to the non-acidic carrier-supported Ir catalysts [18, 48]. Since the primary products generated through the selective cleavage at both the a and b positions can improve the cetane number compared to

the undesirable c cleavage. The (a+b)/c ratio, obtained from the ratio of (2-MC7 + 4-MC7)/2,4-DMC6, is worth to consider to obtain the products with high CN.

The (a+b)/c ratio and conversion of 1,3-DMCH over the catalysts with different K loadings were illustrated in Figure 5.4. In a previous work, (a+b)/c ratio strongly decreased as a function of conversion of Ir/Al_2O_3 while the slight decrease in the ratio was observed on Ir/SiO_2 catalyst [19]. In order to avoid the variation of the ratio as a function of conversion, the W/F (weight of catalyst (g) to flow rate of reaction (ml/h) ratios) among catalysts prepared were varied to compare only the ratios at similar conversion (15-25%). Unlike (a+b)/c ratio comparison, catalytic activity (1,3-DMCH conversion) of different K loadings was compared at the same W/F.

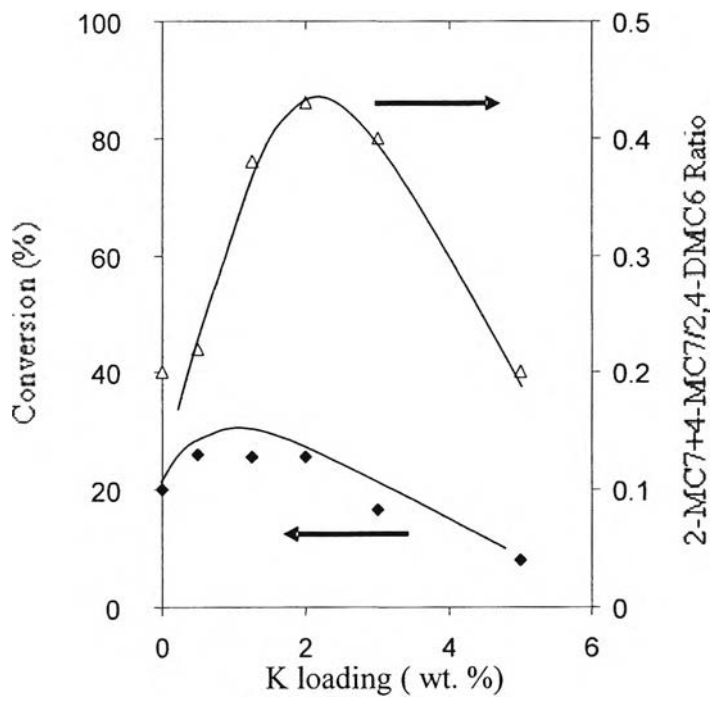

Figure 5.4 Effect of the potassium loadings on 1,3-DMCH conversion and the (2-MC7+4-MC7/2,4-DMC6) ratios. Reactions were carried out at 593 K, 3540 kPa and H_2/HC = 30.

Several interesting trends were observed. Firstly, the (a+b)/c ratio on Ir/SiO_2 is 0.25 which is significantly low compared to statistic number ((a+b)/c = 2). This indicates that the unsubstituted C-C cleavages (c) be more favorable than the substituted C-C bonds (a and b). The preferable to cleavage at unsubstituted positions on Ir metal also found in previous works [3, 19]. In addition, the large ensembles of Ir cluster due to its low metal dispersion on SiO_2 support may facilitate the opening of the ring of C-C bonds at unsubstituted positions. Secondly, It was observed that at low K loading, the presence of K increased the (a+b)/c ratio then the ratio decreased at high K contents (K loading > 2 wt.%). Accordingly well with the increase in metal dispersion which was discussed above. The slight presence of K resulted in the smaller Ir cluster sites that might generate the sites for metallocyclobutane mechanism, consequently, the (a+b)/c ratio was increased as an increase in metal dispersion as shown in Figure 5.3. However, at higher K loadings, the excess presence of K was initiated to block the active sites then the increasing (a+b)/c ratio was inhibited. The block of K at high K loading was clearly observed from the trend of 1,3-DMCH conversion as a function of K loading (Figure 5.4). At low K contents, the conversion of 1,3-DMCH was slightly increased while the conversion was drastically dropped at higher conversion with K loading higher than 2%.

The yield of primary products from the cleavage at substituted positions, 2-MC7 and 4-MC7, and unsubstituted position, 2,4-DMC6, on Ir/SiO_2 and $2K\text{-}Ir/SiO_2$ as a function of conversion of 1,3-DMCH is illustrated in Figure 5.5. It was found that the yield of all products was continuously increased as a function of conversion. However, the increasing yields of 2-MC7 and 4-MC7 products were almost constant at higher conversion. In good agreement with the previous work, (a+b)/c ratio decreased as a function of conversion [19]. The decrease of this ratio with conversion is mainly associated with a faster transformation of the longer-chain (2-MC7, 4-MC7) than the more branched molecules (2,4-DMC6). Interestingly, the yields of primary products on $2K\text{-}Ir/SiO_2$ were higher than that over the unmodified Ir/SiO_2. It is noteworthy that the addition of potassium not only improves the (2-MC7+4- MC7)/2,4-DMC6 but also inhibits the secondary hydrogenolysis which causes the lost of carbon number as well. This finding opens an additional way for modifing ring opening catalysts.

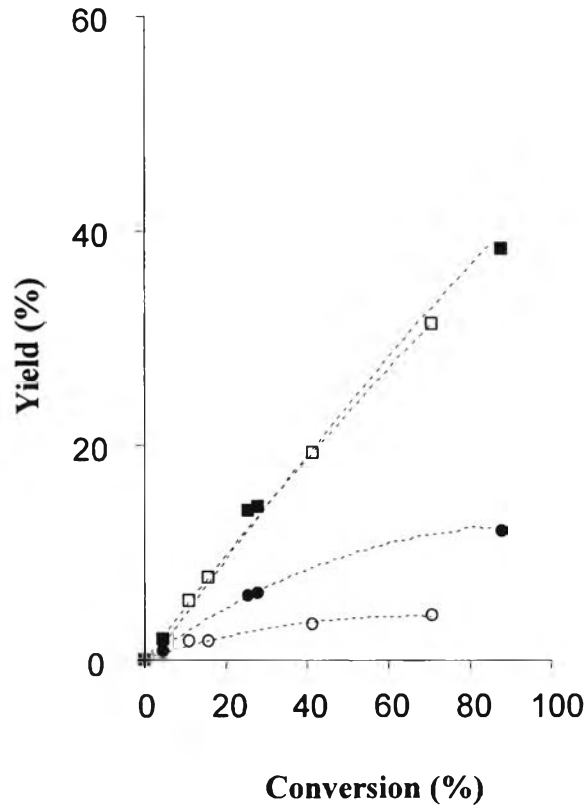

Figure 5.5 Yield of 2,4-DMC6 product on Ir/SiO_2 (□), and $Ir\text{-}2K/SiO_2$ (■), and yield of (2-MC7+4-MC7) on Ir/SiO_2 (○), and $Ir\text{-}2K/SiO_2$ (●) from 1,3-DMCH conversion. Reactions were conducted at 593 K, total pressure of 3540 kPa and $H_2/HC = 30$.

According to Gault (1981), the reaction path involving the metallocyclobutane intermediate would have activation energy higher than that operating the dicarbene intermediate [7]. Therefore metallocyclobutane mechanism could be present only when either the lower-energy dicarbene path was blocked or the metallocyclobutane pathway was selectively catalyzed. We propose that the addition of potassium ions improve the dispersion of Ir on SiO_2 surface. This is reflected in enhancement of the metallocyclobutane adsorption mode and also the inhibition of its secondary hydrogenolysis reaction. Therefore, one can tune the selectivity to ring opening reaction by just changing the potassium loading. We have recently reported that a high-temperature reduction on Ir catalysts is an additional way to hinder this secondary reaction [25]. Simultaneously, a linear reduction of the

ring opening activity with increasing potassium loading is observed. However, the excessive K at high K contents on Ir/SiO_2 causes the decrease in 1,3-DMCH conversion due to the cover of Ir with K. It was found in previous work that the particle size does not affect significantly the ring opening reactions over Ir catalysts, in contrast with the behavior of Pt [7, 49]. However, Ir became more selective toward ring opening at substituted (tertiary) carbon centres as the catalyst became covered by carbonaceous species. It is possible that carbonaceous deposit can hide the true structure sensitivity of these reactions. In the present study, we found strong evidences that the particle size, probably induced by a strong metal-support interaction, plays a very important role in the selectivity to substituted C-C bond rupture compared with unsubstituted C-C bonds under catalytic conditions where low rate of coke formation and negligible catalyst deactivation are obtained.

5.5 Conclusions

The addition of potassium ions to Ir/SiO_2 catalysts produced severe structural and superficial changes that are reflected on its reducibility and the selectivity of ring opening of 1,3-DMCH. The presence of K up to 2%, promoted the reducibility of iridium oxide, probably due to a K-Ir interaction that facilitates the dissociative adsorption of hydrogen, above which potassium contents block most of the IrO_x clusters and inhibit the reduction of the catalyst. Ir dispersions and particle size slightly increased with rising K contents resulting in the non-uniform decorative effect of potassium over Ir particles.

The selective ring opening reaction of 1,3-DMCH over Ir/SiO_2 catalysts can be tuned with addition of potassium ions. The favorable catalytic reaction pathway on Ir/SiO_2 catalysts is in the dicarbene adsorption mode, which is based on the rupture of unsubstituted C-C bonds (secondary-secondary) toward products with high degrees of branching and low CNs. The addition of K ions to Ir/SiO_2 catalysts (2 wt.% of K), markedly improves the metallocyclobutane adsorption mode due to the smaller Ir clusters which facilitate the cleavage of substituted C-C bonds with high cetane numbers and inhibit the continuously hydrogenolysis to secondary products as well.

5.6 Acknowledgements

This work was supported by funds provided by the Oklahoma Center for the Advancement of Science and Technology (OCAST), the Petroleum and Petrochemical College (PPC), Chulalongkorn University, Ratchadapiseksomphot Endowment of Chulalongkorn University for Petrochemical and ConocoPhillips. JRL and FRG acknowledge financial support by ANPCYT, Argentina (Project 06-17492); NSF-CNPq-CONICET collaborative research agreement (CIAM project) and CONICET (Project PIP 6075/05). Portions of this research were carried out at the Stanford Synchrotron Radiation Laboratory, a national user facility operated by Stanford University on behalf of the U.S. Department of Energy, Office of Basic Energy Sciences.

5.7 References

[1] A. Stanislaus, B.H. Cooper, Catal. Rev.-Sci. Eng. 36 (1994) 75.

[2] H. Du, C. Fairbridge, H. Yang, Z. Ring, Appl. Catal. A: Gen. 294 (2005) 1.

[3] G.B. McVicker, M. Daage, M.S. Touvelle, C.W. Hudson, D.P. Klein, W.C. Baird Jr., B.R. Cook, J.G. Chen, S. Hantzer, D.E.W. Vaughan, E.S. Ellis, O.C. Feeley, J. Catal. 210 (2002) 137.

[4] W.C. Baird Jr., D.P. Klein, M.S. Touvelle, J.G. Chen, US Patent 6,589,416 (2003).

[5] R.C. Santana, W.E. Alvarez, J.D. Taylor, E.L. Sughrue, D.E. Resasco, Fuel 85 (2006) 643.

[6] M. Santikunaporn, J.E. Herrera, S. Jongpatiwut, D.E. Resasco, W.E. Alvarez, E.L. Sughrue, J. Catal. 228 (2004) 100.

[7] F.G. Gault, Adv. Catal. 30 (1981) 1.

[8] G. Maire, G. Plouidy, J.C. Prudhomme, F.G. Gault, J. Catal. 4 (1965) 556.

[9] R.J. Fenoglio, G.M. Nuñez, D.E. Resasco, J. Catal. 121 (1990) 77.

[10] D. Teschner, K. Matusek, Z. Paal, J. Catal. 192 (2000) 335.

[11] G. Del Angel, B. Coq, R. Dutartre, F. Figueras, J. Catal. 87 (1984) 27.

[12] F.J. Schepers, J.G. Van Senden, E.H. Van Broekhoven, V. Ponec, J. Catal. 94 (1985) 400.

[13] F. Weisang, F.G. Gault, J. Chem. Soc. Chem. Commun. 11 (1979) 519.

[14] B. Coq, E. Crabb, F. Figueras, J. Mol. Catal. A-Chem. 96 (1995) 35.

[15] T. J. Plunkett, and J. K. A. Clark, J. Calal. 35 (1974) 330.

[16] Z. Karpinski, and J. K. A. Clarke, J. Chem. Soc. Faraday Trans. I 71 (1975) 2310.

[17] J. H. Sinfelt, Calal. Rev. 3 (1969) 175.

[18] M. Boudart, and L. D. Ptak, J. Catal. 16 (1970) 90.

[19] P.T. Do, W.E. Alvarez, D.E. Resasco, J. Catal. 238 (2006) 477.

[20] W.C. Baird Jr., J.G. Chen, G.B. McVicker, US Patent 6,623,626 (2003).

[21] W.C. Baird Jr., D.P. Klein, M.S. Touvelle, J.G. Chen, G.B. McVicker, US Patent 6,586,650 (2003).

[22] W.C. Baird Jr., J.G. Chen, G.B. McVicker, US Patent 6,623,625 (2003).

[23] T.E. Hoost, J.G. Goodwing Jr., J. Catal. 130 (1991) 283.

[24] A.M. Kazi, B. Chen, J.G. Goodwing Jr., G. Marcelin, N. Rodriguez, R.T.K. Baker, J. Catal. 157 (1995) 1.

[25] C. Pedrero, T. Waku, E. Iglesia, J. Catal. 233 (2005) 242.

[26] G.D. Meitzner, E. Iglesia, Catal. Today 53 (1999) 433.

[27] D.G. Barton, S.L. Soled, G.D. Meitzner, G.A. Fuentes, E. Iglesia, J. Catal. 181 (1999) 57.

[28] B. Ravel, M. Newville J. Synchrotron Rad. 12 (2005) 537.

[29] J.J. Rehr, R.C. Albers, Rev. Mod. Phys. 72 (2000) 621.

[30] B. Ravel, J. Synchrotron Rad. 8 (2001) 314.

[31] K. Aika, K. Shimakazi, Y. Hattori, A. Ohya, S. Ohshima, K. Shirota, A. Ozaki, J. Catal. 92 (1985) 296.

[32] J.S. Rieck, A.T. Bell, J. Catal. 100 (1986) 305.

[33] M. Konsolakis, I.V. Yentekakis, Appl. Catal. B: Env. 29 (2001) 103.

[34] C. Wögerbauer, M. Caciejewski, A. Baiker, U. Göbelt, J. Catal. 201 (2001) 113.

[35] K. Foger, H. Jaeger, J. Catal. 70 (1981) 53.

[36] M. Haneda, Y. Kintaichi, N. Bion, H. Hamada, Appl. Catal. B: Env. 46 (2003) 473.

[37] L. Feng, X. Li, D.B. Dadyburjor, E.L. Kugler, J. Catal. 190 (2000) 1.

[38] C. D. Wagner, A.V. Naumkin, A. Kraut-Vass, J.W. Allison, C.J. Powell, J.R. Rumble Jr., NIST X-ray Photoelectron Spectroscopy Database (NIST Standard Reference Database 20, Web Version 3.4).

[39] L.F. Liotta, G. Deganello, C. Leclercq, G.A. Martin, J. Catal. 164 (1996) 334.

[40] L.F. Liotta, A.M. Venezia, A. Martorana, G. Deganello, J. Catal. 171 (1997) 177.

[41] A. Cimino, D. Gazzoli, M. Valigi, J. Electron Spectrosc. Relat. Phenom. 104 (1999)1.

[42] P. Reyes, M.C. Aguirre, I. Melian-Cabrera, M. Lopez Granados, J.L.G. Fierro, J. Catal. 208 (2002) 229.

[43] T. Marzialetti, J.L.G. Fierro, P. Reyes, Catal. Today 107-108 (2005) 235.

[44] A.I. Frenkel, C.W. Hills, R.G. Nuzzo, J. Phys. Chem. B 105 (2001) 12689.

[45] A. Balerna, S. Mobilio, Phys. Rev. B 34 (1986) 2293.

[46] D. Zanchet, H. Tolentino, M. Martins Alves, O. Alves, D. Ugarte, Chem. Phys. Lett. 323 (2000) 167.

[47] M.F. Wilson, I.P. Fisher, J.F. Kriz, Ind. Eng. Chem. Prod. Res. Dev. 25 (1986) 505.

[48] K. Foger, J.R. Anderson, J. Catal. 59 (1979) 325.

[49] J.G. van Senden, E.H. van Broekhoven, J. Vreesman, V. Ponec, J. Catal. 87 (1984) 468.